Chapter 3
Magnets and Magnetic Field Effects

J. Annala, D. Harding, V. Shiltsev, M. Syphers, and J. Volk

3.1 Introduction: Magnets of the Tevatron Accelerator Complex

The magnets of the circular accelerators that comprise the Fermilab complex have contributed to, responded to, and solved a string of accelerator physics issues. Most importantly, the magnets are supposed to generate high quality magnetic fields needed for stable long-term dynamics of the particles circulating in the rings. The quality of the transverse magnetic field $\boldsymbol{B}$ is given by the multipole coefficients in the expansion:

$$B_x + i \cdot B_y = B_0 \sum_{n=0} (b_n + ia_n) \left[\frac{x + iy}{R_0} \right]^n, \tag{3.1}$$

where R_0 is the reference radius (1 in. in the Fermilab accelerators), the pole number is $2(n+1)$ and $b_n(a_n)$ are the normal (skew) multipole coefficients, and b_0 is unity. For example, the multipoles allowed by dipole symmetry, $b_2, b_4, b_6, \ldots$ are designed to be small and would be 0 for a pure $\cos\theta$ coil winding. The precise coil placement, and hence good magnetic field uniformity at the relative level of the multipole coefficients of few 10^{-4}, had the biggest effect on the accelerator performance.

3.1.1 Booster

At the heart of the Booster synchrotron are its combined function magnets (dipole, quadrupole, and sextupole), one focusing and one defocusing on each

J. Annala • D. Harding • V. Shiltsev (✉) • M. Syphers • J. Volk
Fermi National Accelerator Laboratory, PO Box 500, Batavia, IL 60510, USA
e-mail: shiltsev@fnal.gov

V. Lebedev and V. Shiltsev (eds.), *Accelerator Physics at the Tevatron Collider*, Particle Acceleration and Detection, DOI 10.1007/978-1-4939-0885-1_3,

girder [1]. Cycling at 15 Hz in a resonant circuit with a bank of capacitors on each girder, the magnets employ an external vacuum skin around both the core and the coils to avoid eddy currents that would be intolerable in a standard beam tube. While the combined function magnets ensure synchronization between the bending and focusing strength through the acceleration cycle, the ability to adjust the tune is limited and variations in the onset of saturation does change the optics during the cycle.

The original air-core correction dipoles and quadrupoles were distributed about the ring. They were weak magnets only designed to run DC and correct at the injection energy. The expectation was that realignment of the gradient magnets would be used to correct for effects at higher energy, and that less steering range would be needed as the accelerated beam shrank. Correction sextupoles were also included, but due to space constraints they were lumped, not distributed, limiting the resonances they could control. Ramped power supplies were eventually added for some correctors, but power supply and heating limitations prevented running them as aggressively as was desired.

In 2009 installation was completed of new set of corrector magnets, power supplies, and controls, with two dipoles, two quadrupoles, and two sextupoles in a single package on every girder [2]. Combined with more powerful beam instrumentation and analysis, the orbit and tunes can now be smoothed through the entire acceleration cycle. The new quadrupoles are strong enough to move the working point in tune space to a much more favorable location near the half integer. Beam losses have been reduced dramatically [3].

Multi-turn injection of 200 MeV protons into the Booster was initially implemented with an electrostatic septum and a pulsed four-bump. Three to four turns filled the aperture. Improvements over the years included the switch to H-injection, with a stripping foil in the middle of the pulsed four-bump [4]; raising of the injection energy to 400 MeV [5]; and finally the change to a three-bump that improves the incoming trajectory and the lattice of the circulating beam, a change made possible by newly designed pulsed injection dipole magnets [6].

Single turn (or partial turn) extraction employs fast kicker magnets that steer the beam into a pulsed septum magnet. Initially the beam was steered around the extraction septum at both extraction points (transfer to the Main Ring and to the beam dump) using just the DC corrector dipoles. These were later supplemented by a stronger, ramped four-bump at each location. In the course of detailed modeling in 2002, it was recognized that the edge focusing of the bumps was having a seriously negative effect on the optics [7]. Over several years the bump strengths were reduced and one extraction point was eventually completely eliminated by relocating the dump. The opened aperture and reduced optical distortion produced significant improvements in the beam transmission efficiency.

3.1.2 Main Ring

The Main Ring, Fermilab's original top accelerator, served as the injector for the Tevatron from the Tevatron's commissioning in 1983 until the commissioning of the Main Injector in 1998. From 1985 onward it also accelerated the protons to produce antiprotons. The Main Ring was an interesting machine in its own right, holding the honor of being the first separated function synchrotron [8]. By separating the bending and the focusing functions, both the bending field and the focusing gradients could be made significantly stronger than in a combined function accelerator, shrinking the circumference of the ring (or increasing the energy) and reducing the beam size. Using H magnets (rather than the C magnets typical of the day) suppressed half the unwanted harmonic components of the field and allowed a smaller, less expensive magnet. Taking the compactness approach to the extreme, there were two dipole geometries, with apertures tailored to the alternating high and low beta functions in the two dimensions.

The Main Ring also pioneered the use of "Lambertson magnets," iron septum magnets for injection and extraction.

The injection energy from the Booster was high enough that the dipole remanent field was not a major problem as it had been in early synchrotrons, but the remanent sextupole field was always an issue.

During Collider Run I, with the detectors in place, the Main Ring was deformed vertically to make a bypass around CDF [9]. With a significant portion of the ring in a different plane from the rest of the ring, some larger gap dipoles were required to bend the beam vertically, as well as some standard dipoles bussed to run at twice the field with the same current.

3.1.3 Main Injector

The Main Injector dipole magnets are a more conservative design than the Main Ring dipoles to maximize reliability [10]. They are robust and energy-efficient. To maximize the useful aperture, the magnets are curved, following the beam sagitta, rather than straight, like the Main Ring dipoles. Injecting at the same energy into a smaller ring (with a higher field) means that the remanent field is less important. More steel in the yoke and a tapered pole reduces the saturation and minimizes the remanent sextupole field. With two lengths of dipole in the lattice and the magnets designed to run into saturation, it was important to ensure that the ends and the body saturated at the same rate. The 3D modeling tools available were insufficient to design the ends, so multiple iterations of prototyping were required to achieve that goal while also eliminating the sextupole component from the end field [11].

The quadrupoles, too, posed matching challenges. The 2.13-m quadrupoles from the Main Ring were to be reused in the Main Injector, along with new quadrupoles of two additional lengths. For the sake of matching the saturation, so that the magnets could run on the same buses, it was agreed that the Main Ring design would be used, just longer. This required ensuring that the effective lengths of the magnets were in the correct ratios, not the iron lengths [12]. Concern about our ability to get this right led to the addition of trim coils to all the new quadrupoles, but they have not proved necessary. Although the spread in magnet strengths was small enough to ignore, having separate focusing and defocusing buses allowed us to narrow the spread of quadrupole strengths even more by putting the stronger ones on one bus and weaker ones on the other bus.

The Main Ring quadrupoles are only twofold symmetric under rotation, so there is an inherent possibility of an octupole component to the field. Indeed, a fabrication error in the original die for stamping laminations led to a significant octupole in some magnets before subsequent cores were machined to compensate and a new die fabricated. This led to the question of how much octupole was appropriate for the Main Injector. Eventually a balance was struck between the needs of a low octupole for injection stability and a high octupole to help with resonant extraction. During installation the old quadrupoles with high octupole were relegated to beam lines.

After several years of operation, it was agreed that larger aperture quadrupoles were needed at the seven extraction and injection points. To track the other magnets, it was agreed to run the magnets on the same buses as the rest of the quadrupoles. The larger aperture for the same gradient raised the pole tip field and drove the magnets slightly farther into saturation than the rest of the magnets. To compensate, independently powered trim coils were included in each magnet. The end field of these magnets was successfully modeled in 3D, a necessity for matching the integrated gradient of the new magnets with the original quadrupoles below saturation [13].

3.1.4 Antiproton Source

The Debuncher and Accumulator rings of the Antiproton Source required very large aperture magnets with storage ring field uniformity [9]. To keep the magnet cost under control, the yoke size was limited and the magnets designed to run with the steel saturated. The poles were tailored to provide a uniform field at this excitation level, with the consequence that the dipoles develop a severe sextupole component below the design excitation. This became an issue when the Accumulator was used to not just store antiprotons but also to decelerate them for use in an internal target experiment. The quadrupole pole shape was critical, as the good field region extended well beyond the pole tip radius on the center plane.

Several different lengths of one dipole magnet style and of both main quadrupole magnet styles were needed, leading to the requirement that the pole ends be contoured to eliminate contributions to the harmonic components of the field integrals. Several prototype iterations were required on the first quadrupole style, but that solution could be scaled up to the larger quadrupoles.

3.1.5 Recycler

The Recycler magnets are treated in detail in Sect. 3.4. We mention here that use of the low-cost permanent magnets, mostly combined function magnets, was only possible because we needed a low energy storage ring and had a large radius tunnel available [14].

3.1.6 Tevatron

Superconducting magnets define the Tevatron, the first synchrotron built with the technology [15]. Subsequent Sects. 3.2 and 3.3 discuss two subtle aspects of the magnet performance, but the most amazing feature is that they worked at all. Issues that had to be addressed included conductor strand and cable fabrication, coil geometry and fabrication, mechanical constraint and support of the coils, cooling and insulation, and protection during quenches. The coil placement, and hence magnetic field uniformity, had the biggest effect on the accelerator performance [16]. Of the allowed (even) harmonics the lowest (6-pole and 10-pole) could be controlled in a straightforward manner, but the higher harmonics could not be controlled in the simple geometry employed (though only the 18-pole had significant magnitude). On the center plane the field integral is nearly constant out to a radius of about 20 mm, as the various multipoles cancel, but moving vertically from the center plane the field uniformity deteriorates.

The simple end geometry of the dipole coils led to a significant sextupole component in the ends. The design sextupole in the body was adjusted to zero the field integral through the whole magnet. There is some evidence that this longitudinal distribution of sextupole field must be accounted for detailed accelerator modeling [17].

Tevatron superconducting magnets, designed in the 1970s, performed beautifully over the years. The Tevatron experience paved the way for other high energy hadron colliders, like HERA (9 m long, 75 mm bore, 5.3 T dipoles made of NbTi conductor, with Al collar and cold iron), RHIC (simple and economical design of 9 m long, 80 mm bore, 3.5 T dipoles), and LHC (15 m long, 56 mm double bore dipoles operating at 2 K super fluid He temperatures with design field of 8.3 T).

3.2 Chromaticity Drifts and Snapback in the Tevatron and Their Compensation

The Tevatron contains 774 superconducting dipole magnets which operate between 0.66 T (corresponding to 150 GeV) at injection and 4.4 T at the peak design field (1 TeV). The Tevatron dipoles are a single aperture cos(θ) (*cosine theta*) design magnet wound from the so-called Rutherford style cable [18]. The magnet is constructed from an upper and lower half, each consisting of a 35 turn inner coil and a 21 turn outer coil. The cable is composed of 23 strands, each of which contains 2,050 separate 9 μm filaments of NbTi embedded in a copper matrix.

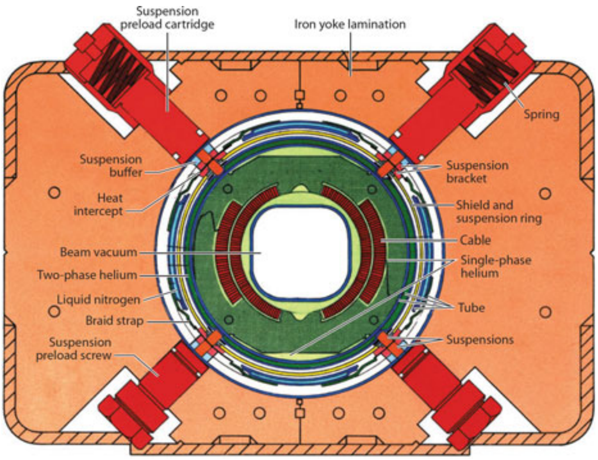

Fig. 3.1 Cross section of the Tevatron superconducting dipole magnet [43]

When the magnets are powered, along with the transport current, there are at least three types of induced currents that can flow in the magnet as well. There are eddy currents between different stands in the cable, and coupling currents between filaments within a strand. Both of these currents decay with time constants of seconds. But there are persistent currents flowing within filaments with extremely long time constants.

The persistent currents exist because of the Meissner effect which causes current to flow on the surface of superconductors in a way that opposes any change in externally applied magnetic field from the interior of the superconductor [19]. In the presence of a changing dipole field, shielding currents form near the surface of the filaments with a magnitude of J_c in a cosine theta pattern that cancels the dipole field in the interior of the filament (Fig. 3.2a). As the external field is increased, the shielding current pattern changes until the filament is penetrated (Fig. 3.2b). This field is known as the penetrating field B_p. The transport current needed to generate the field in real magnets flows at the critical current density in an ellipse interior to the shielding currents (Fig. 3.2c). The transport current is in the same direction as half of the shielding current. Figure 3.1d shows the orientation of four filaments arranged symmetrically around the aperture of a cosine theta dipole magnet, along with their induced dipole moments B_I.

Figure 3.2 shows how persistent shielding currents are set up in a filament to oppose a change in external magnetic field as it (a) starts to rise, (b) fully penetrates the filament, (c) exits with a transport current in the center of the filament and the shielding current induced dipole moments are shown (d) in four filaments symmetrically surrounding a dipole aperture. These induced fields not only have a component opposing the dipole field at the center of the aperture but also have components that lead to a sextupole field, and other allowed (by symmetry) multipoles b_n, $n = 5, 7, \ldots$

The dipole moments induced by the shielding currents can dramatically affect the quality of field in the dipoles. As the transport current reaches its desired current, and then reverses, the shielding currents switch polarity in order to oppose

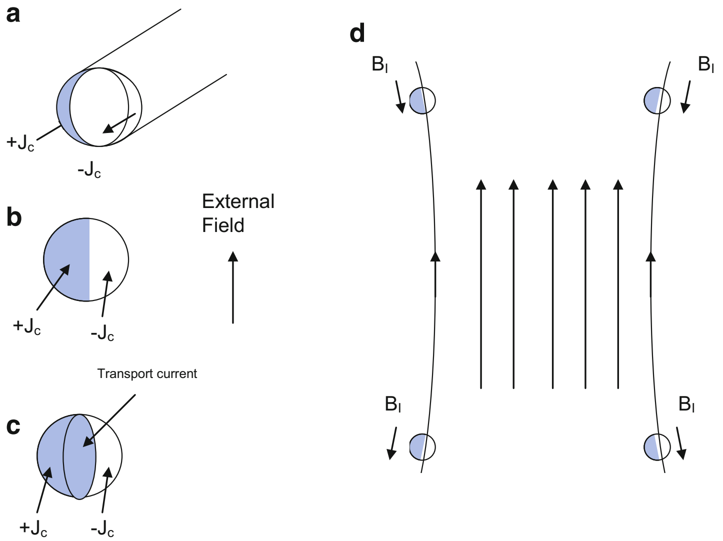

Fig. 3.2 Persistent currents effects in superconducting accelerator magnets: (**a**–**c**) shielding and transport currents in the filament; (**d**) magnetization currents in four symmetric filaments of a dipole coil

the drop in magnetic field. For this reason, the non-dipole fields (in this case—sextupole) have a large hysteretic component. The persistent currents in the superconductor are most dramatic at low field, with currents well below J_c so the transport current stays near the center of the filament allowing for stronger dipole moments from the shielding pattern. If the magnets are held at a fixed excitation, say, at the injection field, the persistent currents and thus the sextupole fields decay with a logarithmic dependence of time. The source of the decay is the resistive redistribution of Interstrand Coupling Currents (ISCC). These coupling currents flow through a complicated pattern in the copper strands and splices, and as they change, the magnetization of the cable decays.

While the phenomenon of cable magnetization, ISCC, and flux creep was documented long before the Tevatron was built, the implications for the quality of magnetic field was not very well predicted. The hysteretic component of the magnetic multipoles in the dipoles was measured by stopping at a given energy and making careful measurements. It was not known early on that the values of the multipoles would drift when a dwell at a given energy was performed, particularly at lower energies. For this reason, the chromaticity sextupoles had to be adjusted differently, as a function of energy, than predicted by magnetic measurements [20].

The initial operation of the Tevatron was a continuously ramping fixed target machine. Since the injection dwell time was only about 1 s long, the changing sextupole fields at the injection plateau were not an issue. When collider commissioning began, it was noticed that the chromaticity $Q' = dQ/(dP/P)$ on the injection plateau would drift by several tens of units, and the rate of change would decrease

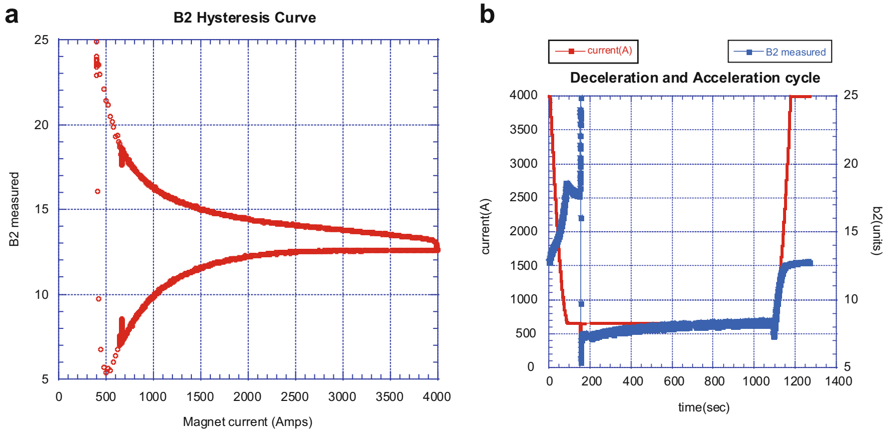

Fig. 3.3 (**a**) Sextupole field coefficient b_2 (multiplied by 10,000) as a function of the current in the Tevatron dipole magnet; (**b**) time dependence of the b_2 and Tevatron bus current for a standard operation cycle

over time. A program was established at the Magnet Test Facility (MTF) to understand the nature of the observed changes in chromaticity. The time resolution of the data acquisition system at MTF was not very good at that point, but it was confirmed that the b_2 component of the dipole magnets would drift away from the hysteresis curve as a function of the log of the time on the injection plateau.

Collider commissioning teams realized that a repeated ramp history would help the chromaticity drift become more repeatable. For these reasons, early collider operation implemented the technique of performing six continuous excitation ramps before stopping at the injection energy. Spending some time at the injection energy then allowed the drift in sextupole fields to be slow enough so that manual chromaticity adjustments could adequately compensate the remaining drift [21].

Figure 3.3a shows the hysteretic b_2 curve along with the drift at the injection level plateaus on both the up ramp and down ramp. The hysteresis curve moves in the counterclockwise direction. This data was taken in 1996 with a data acquisition system that was much better than was available for the original measurements. Figure 3.3b shows the b_2 component of a dipole as a function of time from the end of the deceleration ramp, through the field resetting dip and a 15 min injection porch, followed by an acceleration ramp.

The b_2 drift measurements were made at MTF to verify that operation algorithms were viable. The sextupole field was shown to decay as a function of the log of the time on the injection front porch. There was a faster decay in the first minute, but then both magnet and accelerator measurements displayed the $\ln(t)$ decay. Although the sextupole decay was not explained exactly by theory at the time, the magnet measurement data provided confidence that the operational strategy would be adequate for controlling the chromaticity on the injection porch. The colliding beam sequencer implemented a scheduler function that periodically called

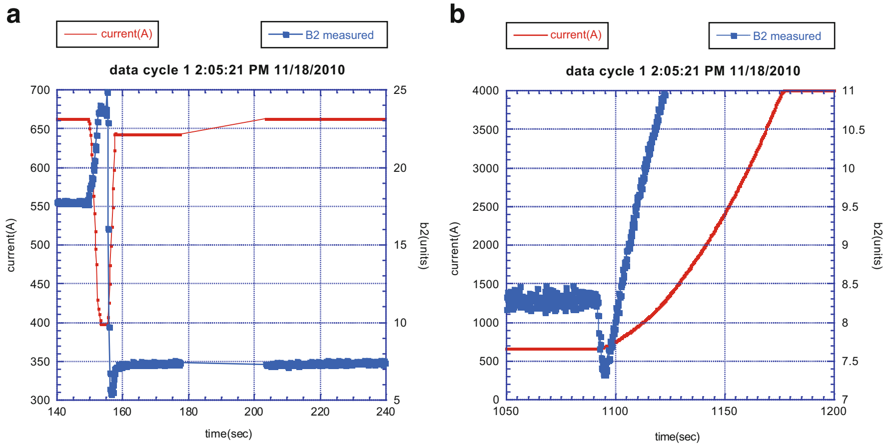

Fig. 3.4 The Tevatron dipole magnet sextupole component b_2 snapback at the end of the back porch (**a**—on the *left*), and at the end of the front porch (**b**—on the *right*)

up the application that loaded the chromaticity tables. Predetermined changes would then be sent to the chromaticity circuits to maintain the desired compensation [20].

The more serious operational issue at that point was the large changes in chromaticity at the start of the energy ramp after a dwell at the injection energy. Measurements showed that the sextupole fields returned to the hysteretic value within the first 30 A of acceleration. A lookup table was developed that calculated an acceleration table based on the length of time spent on the injection porch. This technique allowed acceleration with reduced beam loss and reduced emittance dilution [20].

Figure 3.4a, b shows the b_2 snapback at the end of the back porch, and at the end of the front porch. Again, this data was taken in 1996 with much better data acquisition system than available before the first Collider run.

The Tevatron Collider Run II and the Main Injector era put much more demands on the understanding of dynamic effects in the Tevatron magnets. The plans for maximizing integrated luminosity included the injection of more bunches and the reduction of shot setup times. Procedures involving many pre-cycle ramps and delays on the injection porch were not consistent with efficient luminosity production. Also, the collider plan involved recycling antiprotons, which would require a long dwell time at the injection energy on the down ramp. This extraction dwell would need to vary in time from one store to the next. These considerations necessitated another round of MTF measurements, conducted in the fall of 1996, to understand the effects of different ramp histories. Although the ability to measure and collect harmonic data had improved significantly since the early days of the Tevatron, the power supply regulation at MTF still had limitations and required a modified waveform going into the injection porch to avoid overshoot which would result in reversal of magnetization currents.

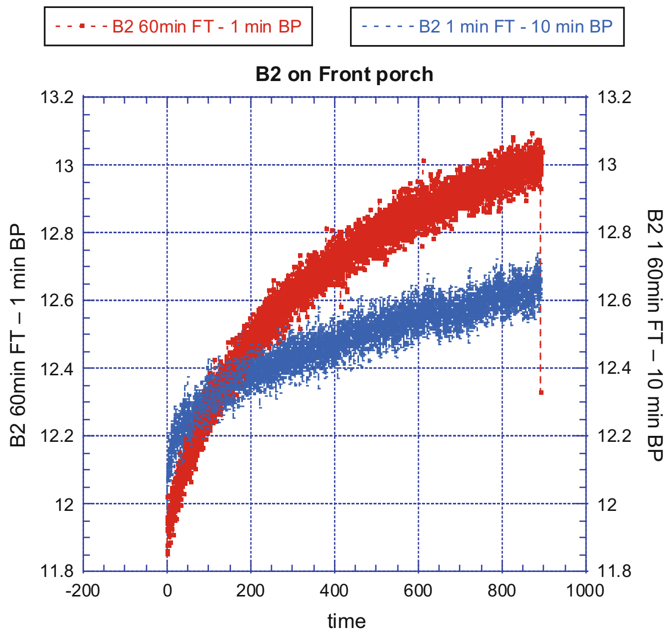

Fig. 3.5 The Tevatron dipole magnet sextupole component b_2 drift at injection after two different current ramps (see details in text)

Figure 3.5 shows the b_2 component of a dipole following two different ramp histories. One of these data sets followed a 60 min flattop with a 1 min back porch. The other data set followed a 1 min flattop with 10 min back porch. These two ramp histories would result in chromaticities that differ by 10 units after the 15 min shown here on the front porch.

Magnet measurements were made to understand how the previous cycles flattop length, as well as the length of the back porch affected the chromaticities that would result on the following front porch. Also, the dependence of ramp energy, ramp rate, and magnet temperature was also investigated. All of these parameters are important parameters in determining the proper compensation for the sextupole drift. Once chosen, the ramp rate, flattop energy, and magnet temperature would not be changing from store to store. It was important to know the functional impact that the flattop length and injection energy dwell times would have on the sextupole fields, as these parameters would necessarily change from store to store. The functional forms of these dependencies were obtained from the 1996 magnet measurements, and then the coefficients were scheduled to be tuned using chromaticity measurements during collider commissioning.

During the very beginning of Collider Run II commissioning, a 30 min pre-cycle and a 90 s back porch was used. Constants for the b_2 drift correction were adjusted to nicely compensate this condition. Since the recycling of antiprotons was not foreseen to take place in the early stages of the run, the need to tune up the drift

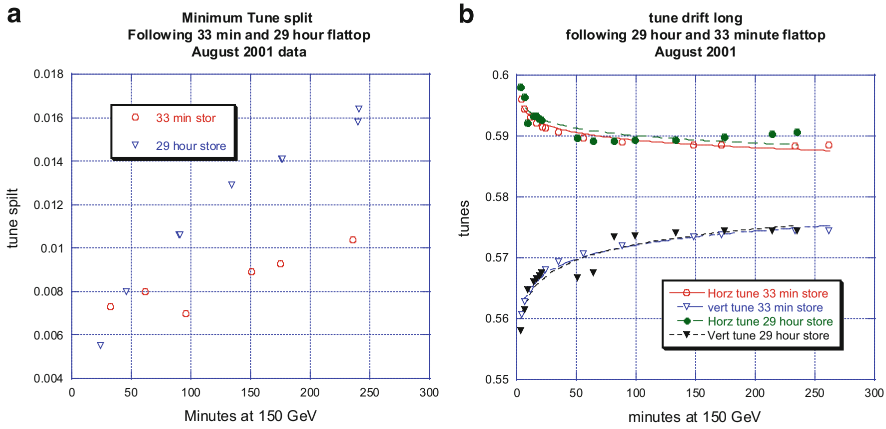

Fig. 3.6 (**a**) The minimum tune split $dQ = |Q_x - Q_y|_{min}$ as a function of time spent at the injection energy of 150 GeV following two different lengths of flattop—29 h and 33 min at maximum energy of 980 GeV; (**b**) same for the horizontal and vertical tune drifts $Q_x(t)$, $Q_y(t)$

compensation scheme for various lengths of back porch times was not required immediately. As commissioning was rushed it was decided to skip this calibration, and instead stay with a pre-cycle with a 30 min flattop and a 90 s back porch before injecting beam. The run continued until 2004 with this mandatory 30 min pre-cycle before each store.

As the Collider Run II began, new phenomenon of tune and coupling drift were also seen. Prior to Run II, only the chromaticity drifted in a way that needed compensation.

Figure 3.6a, b shows the minimum tune split, and tune drift as a function of time on the front porch following two different lengths of flattop. The source of the tune and coupling drift was not understood, but the time dependence of these fields was similar to the chromaticity drift, so the compensation methods were simply expanded to include quadrupole and skew quadrupole correction circuits as well. It is likely that the source of the tune and coupling drifts is a feed-down effect from orbit offsets in the dipoles and correction sextupoles, but this has not been proven with certainty. All of the measured drifts were compensated fairly well for the first portion of Run II as long as the operation included a 30 min pre-cycle, and a 90 s back porch.

Figure 3.7 shows that the chromaticities are compensated very well for the normal operating scenario of a 30 min pre-cycle. The cycle that follows the long 29 h store shows that the drift compensation was not tuned up for that scenario.

New controls mechanisms were also introduced at the start of the Collider Run II to better automate the compensation of these changing fields. The implementation of the correction scheme was coordinated by a central process known as *TCHROM*. This program ran in the background and kept track of the length of flattop, back porch, and front porch for the previous five cycles. *TCHROM* received knowledge of the state of the Tevatron through a state device that was updated by the Colliding

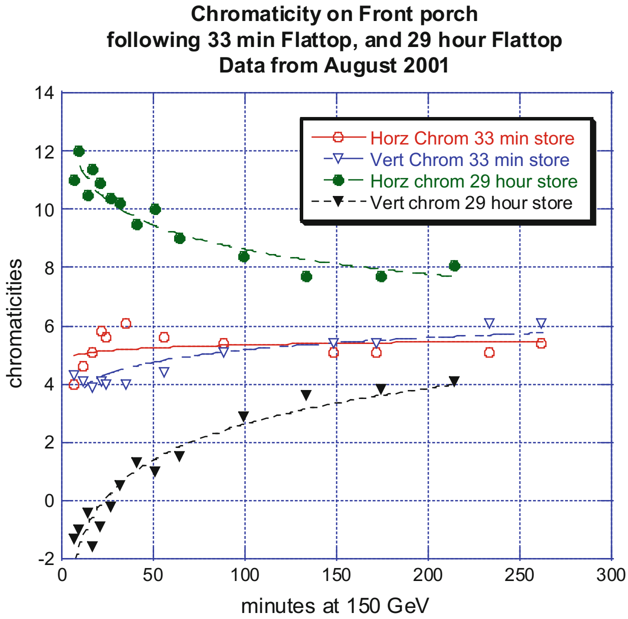

Fig. 3.7 The horizontal and vertical chromaticities $Q'_x(t)$, $Q'_y(t)$ as a function of time spent at the injection energy of 150 GeV following two different lengths of flattop—29 h and 33 min at maximum energy of 980 GeV

Beams Sequencer application program. Before moving to either the front or the back porch, *TCHROM* would calculate compensation curves for the sextupoles, based on the ramp history. The length of time spent on the front or back porch was broadcasted on the machine data link known as *MDAT*. The curves loaded by *TCHROM* played as a function of this time at 150 GeV data frame. At the beginning of the acceleration cycle, the snapback curve is calculated and loaded based on the amount of drift experienced on the front porch. There are a set of 44 constants stored in the database that are used to calculate the proper slope and initial corrections as a function of the previous flattop and back porch length. Since some of the operational flexibility designed into the system was extraneous because of the decision to eliminate recycling of antiprotons, some of the constants are 0, and the equations are more complicated than required for the more simple set of scenarios that are actually used. The controls implementation allows continuous compensation of the field drifts without any interaction from the operators.

There were still occasional issues with compensation of the snapback as a head–tail instability would occasionally arise at the beginning of acceleration causing drastic beam loss. These issues were addressed by running with increased values of chromaticity at the start of the acceleration cycle. This larger than optimal chromaticity did lead to some beam loss, and emittance growth, but these negative effects were fairly minor.

In 2004 there was a very serious effort made within the Fermilab's Technical Division to provide a better model to explain these dynamic effects. Better instrumentation existed by this time so more accurate measurements could be made with much better time resolution. As the behavior of individual magnets was better characterized, a very systematic set of accelerator measurements was planned to implement changes suggested by these measurements. Chromaticity drift measurements were made with various ramp histories. The speed and magnitude of drift were measured as a function of both flattop length and back porch length on the previous cycle. This data along with the magnet measurement data from MTF showing that the dependence on the flattop length saturated at times greater than 1 h lead to great improvements in the compensation equations. The need for a pre-cycle was eliminated for all cases except when the Tevatron ramp was turned off. It was also decided at this time to increase the length of the back porch from 90 s to 5 min as the magnitude and rate of drift on the front porch are less with the longer back porch. The ease of improved compensation was chosen over the decrease in time needed to refill the Collider. The b_2 drift compensation on the front porch always took the form:

$$b_2(t) = b_{20} + m \times \ln[(t + c)/c] \tag{3.2}$$

where both m and c are dependent on the length of the previous flattop up to 1 h.

The 2004 magnet measurements also lead to an improvement in the understanding of the snapback function. Previous to these measurements, the snapback was compensated by a fourth order polynomial function of time from the start of ramp:

$$b_2(t) = b_{2T}\left[1 - \left(t^2/T^2\right)\right]^2 \tag{3.3}$$

where t is time in seconds from the start of ramp, b_{2T} is the total b_2 drift on the front porch, and T is a constant set at 8 s. The function played out completely in 8 s. The improved algorithm was a Gaussian function:

$$b_2(t) = b_{2T} \times \exp\left(-(t/T)^2\right) \tag{3.4}$$

where the length of the snapback compensation T is now a function of the total snapback magnitude b_{2T}:

$$T = [(b_{2T} - 0.061)/0.0682]^{1/2} \tag{3.5}$$

The exact values of the constants in the above equation were obtained by careful beam measurements at the beginning of the ramp. Tune spectra were collected as rapidly as the spectrum analyzer would allow on ramp cycles with different RF frequency offsets. The tune data were collected on three separate ramp cycles with identical ramp histories, but with RF frequency offsets of 0, +40 Hz, and −40 Hz and that was used to calculate the actual chromaticity during the snapback—see Fig. 3.8 from [22].

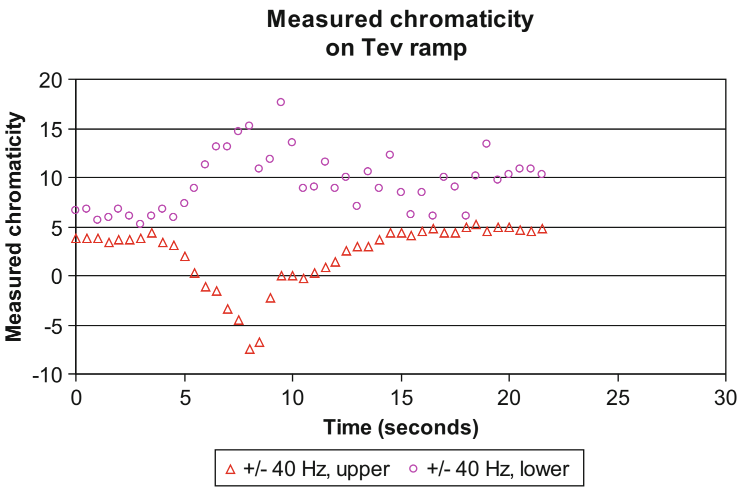

Fig. 3.8 Time evolution of the vertical and horizontal chromaticity values at the beginning of the current ramp. The scatter in data results from difficulty in discerning the correct tune line on the spectrum analyzer when the chromaticity is large

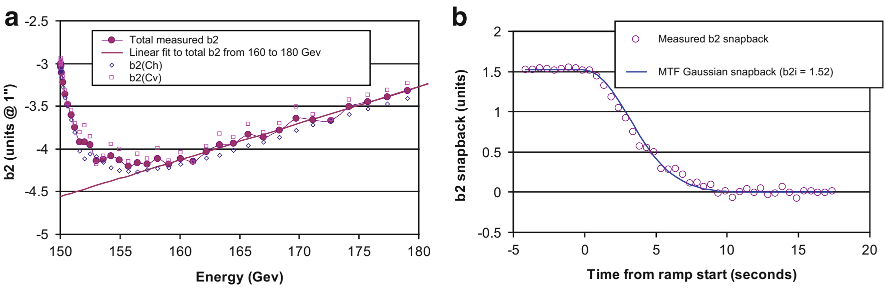

Fig. 3.9 (**a**) The average Tevatron sextupole field component b_2 as a function of energy at the start of the acceleration ramp calculated from the actual chromaticity measurements (see Fig. 3.8); (**b**) Comparison of the b_2 snapback determined from the beam measurements and the snapback calculated on the base of the MTF magnet measurements

Figure 3.9a shows the actual chromaticity measurements converted to units of b_2 as a function of energy at the start of the acceleration ramp. Figure 3.9b shows the agreement between the beam measurements, and the snapback calculated at MTF. One unit of b_2 is equivalent to 26.4 units of horizontal chromaticity and -24.1 units of vertical chromaticity.

The change to a Gaussian compensation curve improved the correction by a couple of units of chromaticity for an 8 s snapback, if the duration of the snapback compensation was unchanged. But the new knowledge that the length of time for the duration of the snapback was a function of the total drift on the injection porch was allowed improving the correction by another 2 units of chromaticity (see Fig. 3.10).

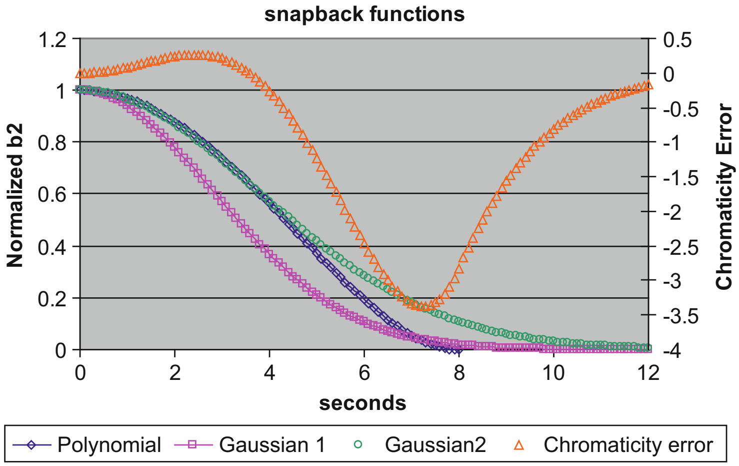

Fig. 3.10 Compensation curves are shown for the early polynomial correction, a Gaussian correction without a modification in the time of the curve, and the final Gaussian correction with a typical time compensation time. Also shown is the chromaticity error resulting from the earlier polynomial correction assuming the *Gaussian2* correction is perfect

Implementing this change allowed the chromaticity tables during acceleration to be changed to values that produced lower chromaticities without the danger of resulting in negative values and a head–tail instability. This resulted in less beam loss and emittance growth during the ramp. Drift compensation tables are calculated for the extraction porch every cycle, but these curves have not been needed since deceleration of antiprotons was eliminated from the operational scenarios.

3.3 Coil Creep and Skew Quadrupole Field Components in the Tevatron

During the start-up of Run II of the Tevatron Collider program, several issues surfaced which were not present, or not seen as detrimental, during Run I. These included the repeated deterioration of the closed orbit requiring orbit smoothing every 2 weeks or so, the inability to correct the closed orbit to desired positions due to various correctors running at maximum limits, regions of systematically strong vertical dipole corrections, and the identification of very strong coupling between the two transverse degrees-of-freedom. It became apparent that many of the problems being experienced operationally were connected to a deterioration of the main dipole magnet alignment, and remedial actions were undertaken [23]. However, the alignment alone was not enough to explain the corrector strengths required to handle transverse coupling.

With one exception, strong coupling had generally not been an issue in the Tevatron during Run I. Based on experience with the Main Ring, the Tevatron was designed with a very strong skew quadrupole circuit to compensate any quadrupole alignment and skew quadrupole field errors that might present themselves. The circuit was composed of 48 correctors placed evenly throughout the arcs, eight per sector, evenly placed in every other cell. Other smaller circuits were installed but not initially needed or commissioned. These smaller circuits were composed of individual skew quadrupole correctors on either side of the long straight sections. These circuits were tuned by first bringing the horizontal and vertical tunes near each other. The skew quadrupoles were then adjusted to minimize tune split, usually to less than 0.003. Initially, the main skew quad circuit (designated T:SQ) could accomplish this global decoupling with only 4 % of its possible current, and the smaller circuits were not required at all. The start-up of Run Ib was complicated by what was later discovered to be a rolled triplet quadrupole magnet in one of the Interaction Regions [24, 25]. This led to a reduction in luminosity of nearly 50 %, as well as operational confusion until it was uncovered.

By the time Collider Run II began, the current needed on the main SQ circuit had increased to 60 % of its maximum value. Some of the smaller circuits were also needed to fully decouple the tunes. With this history, several studies were performed early in Run II to search for strong local coupling sources like the triplet quadrupole, but without success. The strong corrector settings were indicative of a much larger problem than a single-rolled magnet, and the locality of the error was hard to deduce from the setting of a global correction system. Several possible reasons for the increase in coupling were investigated.

3.3.1 Strong Systematic Steering Correction

In late 2002 regions of the Tevatron were found to contain vertical steering magnets whose average strength was required to be nonzero in order to produce a smooth trajectory as seen on the Beam Position Monitors. Compared to the 0.7 μrad average horizontal steering corrector strength, the vertical correctors had a ring-wide average of about 16 μrad, and areas of the Tevatron had strengths of 70–90 μrad averaged over distances of 400 m or so. At 1 TeV, the maximum strength of a corrector is a little more than 100 μrad, so the available correction for general beam steering was limited in these locations. The interpretation of this effect was that these areas contained magnets which were systematically rolled toward the inside of the tunnel. This was verified by magnet roll angle measurements performed in October 2002 and January 2003.

The rolled dipoles and systematic corrections produce a “scalloped” vertical trajectory through the bending regions [26]. Although the distributed beam position monitors read zero displacements, the beam actually underwent ~0.5 mm excursions through these regions, assuming the magnets were rolled about the beam pipe axis. The fact that they are actually rolled about a different axis closer to the floor meant that the beam trajectory was closer to 1 mm or more from the center of the magnet coil.

Since the Tevatron dipoles have a sextupole component, a systematic vertical offset feeds down into a coupling term between the horizontal and vertical motion. The sextupole component is also known to vary as the logarithm of time due to persistent current effects at low magnetic fields; hence the coupling varies with time accordingly. This effect might explain some of the observed tune drift behavior during the Tevatron injection process, but was not nearly enough to explain the large skew quadrupole corrector settings.

In addition to the transverse coupling generated by orbit feed-down through rolled dipole magnets, the coupling due to observed quadrupole magnet rolls was calculated. Taken together, these effects were strong enough to explain a correction of the minimum difference between the two transverse tunes of amount $\Delta Q = |Q_x - Q_y| \approx 0.03$. However, the setting required of the main skew quadrupole correction circuit to decouple the Tevatron was indicative of an order of magnitude larger coupling.

3.3.2 Injection Experiment

Beam studies were conducted to see if a local source of the coupling could be pinpointed. All of the skew quadrupoles were set to 0, and then beam position data were collected for the first several turns before dumping the beam. The beam was then mis-steered in the horizontal plane, and orbit data again collected on the first several turns. The orbit differences are shown in Fig. 3.11. The purely horizontal error coupled fully into a vertical error in about 1.5 turns, and then back into the horizontal plane in another half period [27].

The fact that the coupling builds up gradually and not at a few localized sources is indicative of a uniformly distributed source of skew quadrupole fields. The 3-turn period of the coupling is consistent with a tune split of order $\Delta Q \approx 0.3$. It was quickly noted that a systematic skew quadrupole term, $a_1 \equiv (\partial B_x/\partial x)/B_0$, would account for this behavior, and would need to be of order $a_1 = 1.5 \times 10^{-4}$ in.$^{-1}$, or 1.5 “units” [28].

While regions of rolled dipoles existed at the time, the possibility that a systematic roll of the main quadrupoles could give rise to the coupling problem was unlikely, as the focusing and defocusing quadrupoles would have to be rolled in opposite directions. Direct roll measurements of the quadrupoles performed in 2002 also disproved this as the strong coupling source.

3.3.3 Mechanical Issues

In January 2003, as plans were being made to correct the rolled Tevatron dipoles discussed above, the question arose of ensuring that the cryostat and coils moved with the warm iron magnet yoke. The hope was that the magnets could be realigned without disturbing the cryogenic and vacuum connections between adjacent magnets.

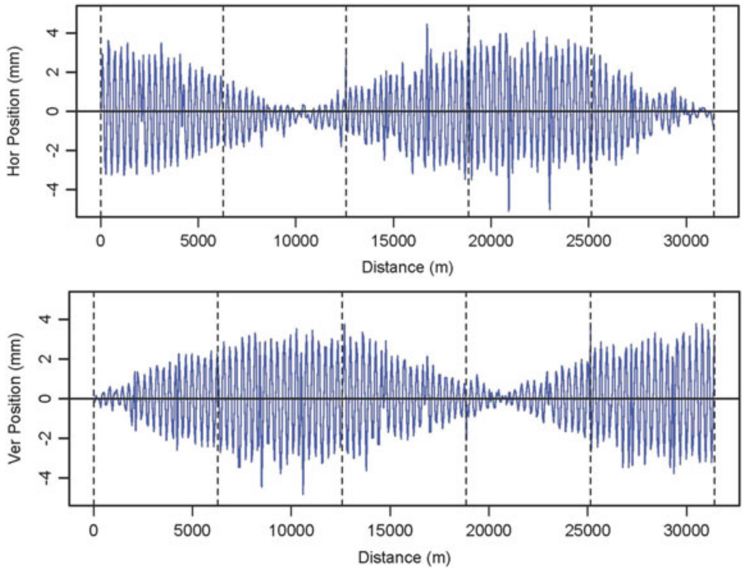

Fig. 3.11 An initial horizontal steering error couples completely to the vertical plane. This data set, taken in February 2003, had all skew quadrupole correctors turned off. *Top*—horizontal beam positions, *bottom*—vertical beam position after traveling distance *s*

The Tevatron dipole cross section is shown in Fig. 3.1. A warm iron yoke surrounds the cryostat tube and the collared coil within it. The collared coil is supported in the cryostat at nine stations down the 6-m length of the magnet. At all but the center station the support is two rectangular blocks of the G11 epoxy-glass plastic, called "suspensions," approximately 8.5 mm × 6.4 mm × 17 mm, aligned with each other, one between the outer cryostat skin and the heat intercept at liquid nitrogen temperature and the other between the heat shield and the phase single helium tube. These suspensions are arranged in grooves that allow the whole cryostat to move longitudinally relative to the yoke as it is cooled. At the middle station more robust G10 tubes, known as "anchors" support the cryostat, anchoring the center against both longitudinal motion and rotation relative to the yoke (a bane of earlier designs of the magnet).

At each station four supports are located at the 45° points. A screw or suspension cartridge through the yoke at each of these points contacts the outside of the cryostat. This allows the cryostat to rest stably in a cradle formed by the lower two screws ("bolts"), while being held down against those supports by two preloaded upper suspensions, spring-loaded cartridges known as "smart bolts." The preloaded springs maintain a force as the collared coil and cryostat shrink during cool down.

As discussed in more detail below, the magnets had been designed to allow adjustment of the coil position while the magnet was cold by adding and removing shims from the cryostat suspension system. During production this feature was used as a standard procedure to compensate for fabrication tolerances and mechanical differences between the top and bottom coils. A depth gauge can be used to measure the distance from the top of the cylinder to the top of the cartridge, a distance that became known as the "lift." For example, as the magnet was cooled, the collared coil shrank, the outer skin of the cryostat deformed slightly, the springs pushed the cylinders inward, and the lift increased. In 2002, lift measurements seemed to have potential for monitoring the movement of the cryostat relative to the yoke during magnet realignment.

To assess the viability of making these measurements in the tunnel and to check the stability of the cryostat over time, technicians measured 18 magnets during a day in February 2003 when the accelerator was down for maintenance. The original (paper) production records of the magnets were retrieved from off-site storage and the lift measurements extracted. By the end of February the data had been analyzed and it was apparent that in those 18 magnets the coil had systematically dropped vertically approximately 0.11 mm relative to the yoke. After a bit of thought it was realized that this was probably due to "creep," slow inelastic deformation under pressure, in the G11/G10 blocks that support the coil within the cryostat. The sizing of the G11 suspensions was a balance between mechanical strength and the heat load a larger conducting cross section would present. The stability of the blocks was the subject of a study at the time [29]. One participant remembers the 1980 guidance to "design the magnets to last for 20 years" [30].

The measured change was enough to produce a skew quadrupole component in the field of about $a_1 = 1.5 \times 10^{-4}$ in.$^{-1}$ or 1.5 "units." If every Tevatron dipole had developed with age a skew quadrupole component, that would explain the observed effects the beam coupling effects.

3.3.4 Mechanical Issues

Once the Tevatron dipole magnets were considered to be the main source of the coupling, further verifications were performed using beam measurements as well as magnet measurements. During Run I, upgrades of the low beta insertions required some of the existing spool pieces to be replaced with new devices. As a result, six skew quadrupoles were lost, one upstream and two downstream of each interaction point. Thus, while the distribution of a_1 was essentially uniform around the ring, its correction was no longer uniform.

The evenly spaced coupling errors from the dipole magnets were being compensated with correction circuits that now had gaps at two locations. Since the horizontal and vertical phases advance differently through a half cell, the main skew quad circuit was not able to fully correct the coupling caused by the distributed coupling errors. Powering the small skew quadrupole circuits near the straight sections in conjunction with the main circuit was necessary to fully minimize the global coupling. At injection, the most effective of the smaller circuits was the one surrounding the A0 straight section, and the skew quad at location A49 was also utilized. Since the smaller circuits consisted of only one or two elements, the strength of these correctors needed to be quite high to completely minimize the global coupling. Under these conditions, the nonuniformity of the coupling correction consisted not only of the gaps in the main circuit but also the additional skew quadrupoles around A0 and at A49.

3.3.5 Vertical Dispersion

A horizontal offset in a skew quadrupole results in a vertical kick. A horizontal offset due to momentum in a skew quadrupole will therefore result in a vertical kick, creating vertical dispersion. Given the value of horizontal dispersion at the location of the skew quadrupole elements around A0 and at the gaps in the main skew quad circuit, a significant vertical dispersion resulted. The dispersion at A49 was very small so that a skew quadrupole there did not contribute to the vertical dispersion.

The dispersion can be measured easily by changing the RF frequency and recording the resulting orbit difference. Figure 3.12 shows the dispersion measured in both planes at the injection energy of 150 GeV in early 2002.

The value of the horizontal dispersion function oscillates in the arcs of the Tevatron between about 1 and 5 m, and vanishes at the interaction points, in agreement with the design lattice. By design, the vertical dispersion should be 0, though a small "residual" vertical dispersion is always present due to various error sources, and would be expected to have a random distribution with peaks of approximately 0.2 m in the Tevatron. The vertical dispersion measurements, however, showed a fairly coherent dispersion wave of up to 0.8 m that is largest between D0 and A0, smaller between B0 and D0, and very small between A0 and B0. This pattern is consistent with calculations based on coupling errors due to the strong correction circuits at A0 and A49, and the gaps in the correction circuit near B0 and D0. The vertical dispersion was near maximum value at the injection point at F0 leading to an emittance increase of up to 1π mm mrad or more for injection of coalesced proton bunches [31].

3.3.6 More Magnet Data

The lifts of an additional sample of 66 magnets were measured in the tunnel during a subsequent short maintenance period, confirming the original distribution. Similar changes in the coil position were measured in spare dipoles that had not been in service. The original calculations from the production era were repeated, affirming the linear relationship between displacement and skew quadrupole error term, $a_1 = k{\cdot}y$, where k is 10.6 units/mm. Several spare dipoles were magnetically measured [32], confirming that the long-term change in lift was reflected in the expected change in skew quadrupole. The amount of its life that a magnet had spent cold or

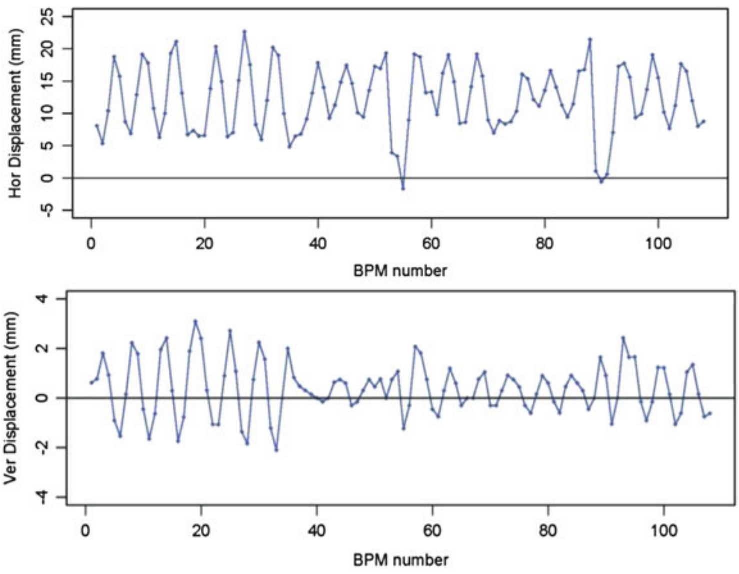

Fig. 3.12 The horizontal (*top*) and vertical (*bottom*) orbit difference given by 500 Hz RF frequency shift, taken in early 2002. The position shift at a BPM is proportional to the dispersion at that location $(x, y) = 3.4$ [mm] $D_{x,y}$ [m]. The vertical displacements clearly show a coherent pattern

warm did not seem to affect its creep. Many more magnets have since been measured during the major shutdowns of 2003 and 2004. The distribution of lift change, averaged over each magnet, is plotted in Fig. 3.13. The average shift of about 0.14 mm (0.0055″) is clearly seen, as is the breadth of the distribution. The difference between the average left and right lift changes is centered on 0, indicating no lateral movement.

The spring force in the smart bolts is sufficiently greater than the weight of the cryostat that we take the compressive force on the upper and lower suspensions to be equal and interpret the change in lift to be creep equally distributed between the upper and lower sets. Note also that an equal creep all around results in a change in the coil position that is the vector sum of the creep in the two lower suspensions.

3.3.7 Magnet Field Correction During Production

When there is any asymmetry in the coils of a conductor-dominated dipole magnet, an error field is produced, which we characterize by the coefficients of its harmonic decomposition. For convenience we normalize the error field to the central field, take the reference radius to be 25.4 mm, and quote the coefficients in “units” of parts in 10^4. This means that if we can bring the coefficients into the range of unity, the magnetic field will be acceptable over the useful aperture of the magnet.

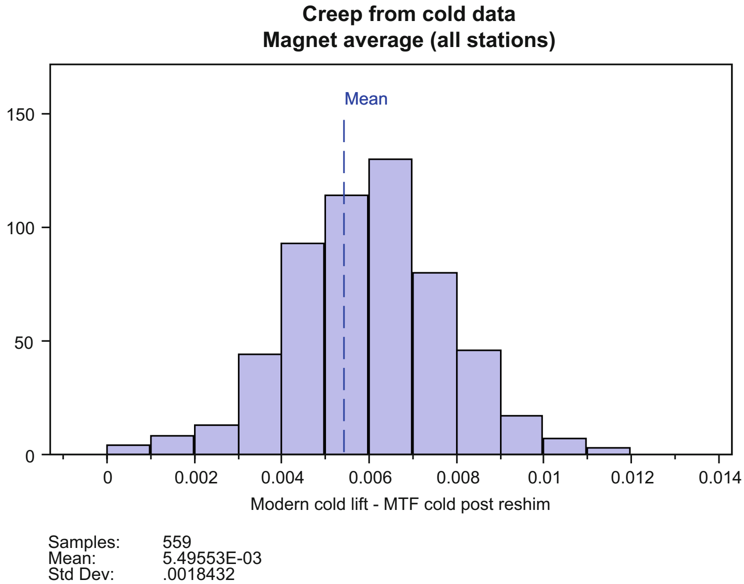

Fig. 3.13 Distribution of the "lift" changes from production to now due to creep (indicative of vertical displacement of the cold mass w.r.t. the magnet iron yoke, in inches). For each magnet the change is averaged over all accessible stations

The asymmetry may be in the geometry of the coils, in their placement in the yoke, or in the superconducting cable. Of particular concern here is the fact that a normal (skew) quadrupole term is produced by the horizontal (vertical) displacement of the coils from the center with a linear dependence. By adjusting the cryostat and collared coil position in the yoke, the quadrupole components of the field could be eliminated or canceled during production.

During assembly brass shims were placed on the end of all four bolts at each station to roughly center the coil in the yoke. Each of the almost 1,000 (including spares) production magnets was measured in detail [33]. After quench testing, the harmonic components of the magnet field integral were measured at one current and the magnet was shimmed according to the guidance provided by a computer calculation. The cryostat support system described above allowed these adjustments while the magnet was cold. While the magnet was still on the test stand, one opposing pair bolts were removed at a time, shims were shifted from one bolt to the other to reposition the coil, and the bolts screwed back in. The magnet was then measured at multiple currents on both the up and down ramps. This data set includes every magnet and provides a measurement of the entire magnet field integral. The specification called for both quadrupole components to be adjusted, if needed, to be within 1 unit of zero. If the first try did not succeed, a new shim adjustment could be calculated and the process repeated. Figure 3.14 shows the final distribution of the skew quadrupole component.

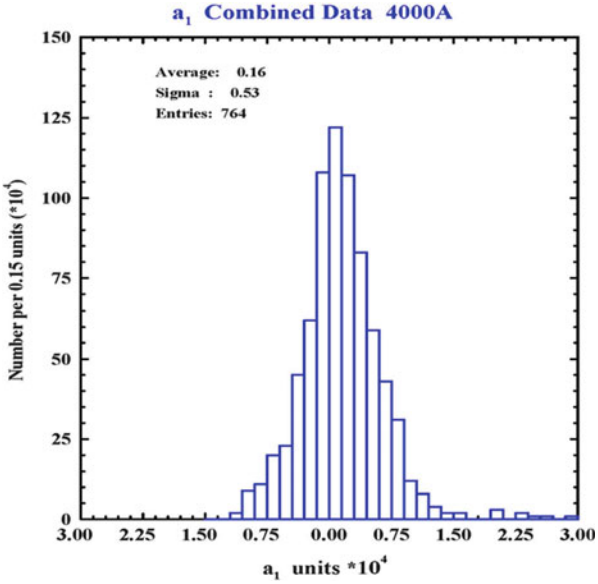

Fig. 3.14 Final distribution of skew quadrupole in Tevatron dipoles after production shimming

3.3.8 The Reshimming Plan

During production the results of shimming could be verified immediately. This would not be possible during reshimming in the tunnel. Examination of the production lift data quickly led us to the conclusion that it was not sufficiently reliable on a magnet-by-magnet basis to warrant the effort of individual treatment. Measuring the lifts of each magnet, comparing them with the production values, and reshimming accordingly would have been fraught with possibilities for error. Instead, it was decided to treat all magnets as though they had changed by the same amount. The addition of a standard shim 3 mil or 0.076 mm (1 mil is one thousandth of an inch, 0.025 mm) was agreed upon, raising the coils by 2.12 mil (0.054 mm).

With 774 dipole magnets in the Tevatron, and with 18 shim locations per magnet, it was clear that to fix the problem completely would take significant tunnel access time. Trial runs above ground had shown that although the job in the tunnel was tedious, requiring the technicians to crawl over the magnets in tight quarters, a crew of three could comfortably reshim two magnets per day. It was not clear, however, how many exceptional cases would arise requiring extra time and how well the crews would hold up with time, even with careful ergonomic planning. So, given some uncertainty in the effectiveness of the reshimming operation, the limited resources, and the uncertainty in the amount of time to reshim the magnets, we decided to start with a modest correction program. We initially focused on the region where the regularity of skew quad correction system had been interrupted, with the idea that the balance of the ring could be reshimmed in future maintenance periods.

For the first run in the fall of 2003 we chose to reshim 106 magnets divided between the two sides of each intersection region, the areas that had their skew correction systems disrupted. After this work, the accelerator performance was significantly improved, so another 12 magnets were reshimmed in March 2004 during a 1-week shutdown. The next major period of repair was the following fall (September–November 2004) when 412 dipoles were reshimmed. This set of dipoles consisted of magnets that were at least four dipole locations from the nearest main skew quadrupole corrector. The performance continued to improve after the second repair, and the remaining 244 dipoles were adjusted in early (March–April) 2006.

The sensitivity of the operation led us to augment our usual quality assurance procedures with more formal analyses [34]. The sheer volume of measurements, 18 lift measurements for each magnet before and after the reshimming, required extensive above ground monitoring in addition to the teams of technicians in the tunnel.

3.3.9 Accelerator Performance Improvements: Reduced Skew Quadrupole Correction, Reduced Vertical Dispersion, Reduced Emittance Growth at Injection

After each round of reshimming the required current in the main skew quadrupole correction circuit decreased, giving clear indication that the reshimming was reducing the skew quadrupole component in the dipoles—see Fig. 3.15 (note that the current is negative and 0 is at the top of the plot). There is only a small change after the first stage, which only addressed the regions where the main skew quadrupoles had been removed. The two stages that addressed the regions covered by the main skew quad circuit were directly effective. The current on the injection “front porch” has decreased by a factor of 6. All other skew quad circuits were reduced to near 0 at the injection energy by the first stage of reshimming, as expected. Stronger coupling corrections are needed at high energy.

The vertical dispersion has been reduced with each phase of the reshimming. A dispersion measurement from 2011, shown in Fig. 3.16, can be compared with the starting dispersion measurement from 2002, shown in Fig. 3.12. The 2011 measurement shows vertical closed obit changes of about 1 mm, oscillating with roughly constant amplitude, where in 2003 the amplitudes varied around the ring, peaking at over three times this amount.

Most importantly, the emittance growth at injection due to the mismatch between the optics of the rings and the injection lines has also decreased dramatically. Figure 3.17 shows the proton injection emittance growth by store number spanning the first two major reshimming periods. Where in early 2003 the rms emittance growth was typically over 1.3π mm mrad, immediately after the first round of reshimming the emittance growth dropped to 0.6π mm mrad. The second major round of reshimming reduced the growth by another 0.4π mm mrad.

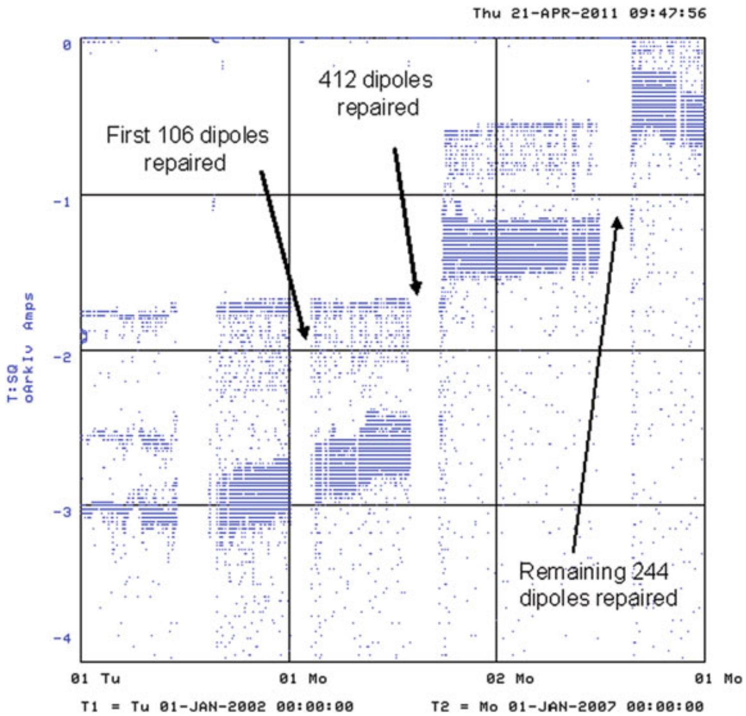

Fig. 3.15 Six-year plot of current in main skew quadrupole circuit T:SQ. The *darkest bands* show the current during the time on the “injection porch”

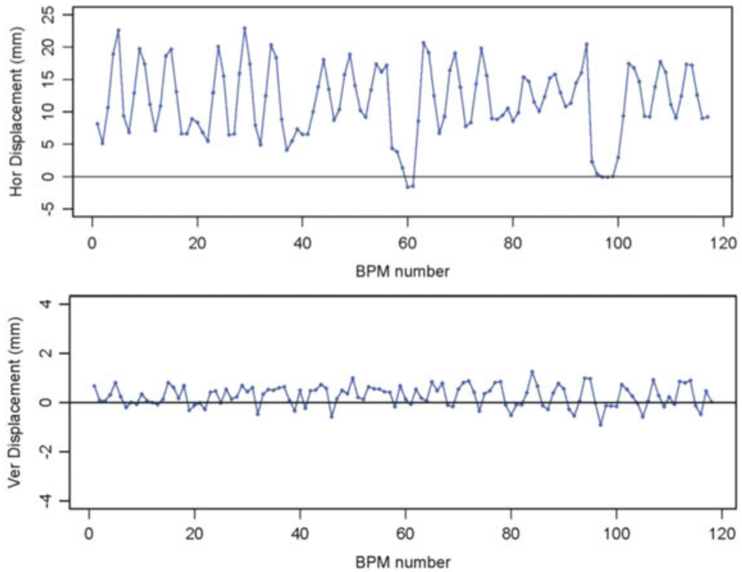

Fig. 3.16 Results of dispersion measurement made in 2011 to be compared with the 2002 measurement shown in Fig. 3.12

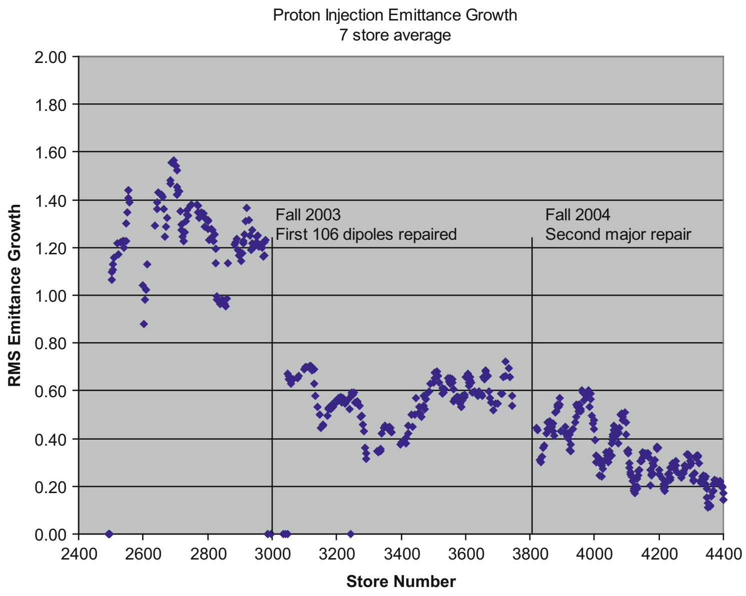

Fig. 3.17 Seven-store average of the proton injection emittance growth spanning the period of the first two major repair periods (April 2003–October 2005)

The reshimming has had an indirect benefit as well. With the major sources of coupling removed, other sources (such as two rolled arc quadrupoles) could be identified and the entire Tevatron lattice restored closer to its design. Correspondingly beam measurements have become much cleaner and easier to interpret, greatly enhancing the operation of the collider.

3.3.10 Summary

Many issues plagued the ramp-up of luminosity during Run II of the Tevatron collider program. While adjustments of the global coupling of the accelerator using a systematic skew quadrupole magnet circuit could allow the operators to place the betatron tunes at desirable settings, other confusions ensued. For example, horizontal corrections that seemed to induce vertical oscillations hampered the commissioning of beam damper systems, and unexplained emittance growth—particularly in the vertical degree of freedom—upon injection was difficult to track down. The required settings of the quadrupole corrector circuit indicated that large sources of coupling were present—and beam measurements soon verified that the source was everywhere. Independently but in parallel, the explanation emerged from both the interpretation of beam measurement data and of magnet measurement data taken in the tunnel—the Tevatron dipole magnets were the source and a mitigation scheme was required. The coils of essentially every dipole magnet in the tunnel were shimmed to re-center them in their iron yokes. The process, which took careful planning and special training, was strategically implemented over a period of years during planned shutdowns of the collider program, restoring the Tevatron to its 1980s state of small residual coupling, both globally and locally.

3.4 Recycler Ring Permanent Magnets Design and Stability

The Recycler was designed as a fixed 8 GeV kinetic energy antiproton storage ring [14]. It is the first ever large-scale (3.3 km circumference) accelerator for high energy physics research built with permanent magnets instead of usual electromagnets. It is located in the Main Injector tunnel directly above the Main Injector beamline, near the ceiling, and consists of 362 gradient dipole magnets, and 109 quadrupoles, 8 mirror magnets, and 5 Lambertson magnets. There are four types of gradient magnets: focusing and defocusing, with pole lengths of 3.1 and 4.5 m. Each has different quadrupole and sextupole fields (see Table 3.1). The basic design consists of precision-shaped pole tips and pole spacers with strontium ferrite bricks on the outside of the poles [35, 36]. The entire package is surrounded by 19 mm (0.75 in.) thick flux return. A typical cross section is shown in Fig. 3.18. A standard SrFe brick size of 101.6 mm by 152.4 mm by 25.4 mm (4 in. by 6 in. by 1 in.) was used. The field axis was orientated along the 1 in. thickness. Two bricks were used on each side of the pole pieces to generate the required field.

The variation of the magnetic field of Strontium ferrite with temperature [37] was carefully measured by freezing the magnet to 0 °C then heating the magnet to 40 °C and allowing it to cool. During this process the magnetic field was continually measured with a Morgan (rotating) coil. A least square fit to the data gave the temperature variation B-field coefficient of about −0.2 %/°C. This intrinsic temperature coefficient of the ferrite material is canceled by interspersing a “compensator alloy” between the ferrite bricks above and below the pole tips—see Fig. 3.19. The compensator is an iron-nickel alloy Ni (30 %) Fe (70 %) with a low Curie temperature in the range of 40–45 °C and therefore its permeability depends strongly on temperature. Thin strips of the alloy shunt away flux in a temperature-dependent manner which can be arranged to null out the temperature dependence of the ferrite. The degree of temperature compensation is linearly related to the amount of compensator material in the magnet. Thus the degree of compensation can be “fine tuned” to the required accuracy by adjusting the amount of compensator at the ends of the magnet in a manner similar to the strength trimming with the ferrite. For example, a 20-fold reduction of the temperature coefficient (from 0.2 to 0.01 %/°C) requires that the amount of compensator in the magnet be adjusted correctly to 1 part in 20. This poses no difficulties for

Table 3.1 Recycler gradient magnet parameters

Magnet	Central field (kG)	Bdl (kG/m)	Quadrupole units	Sextupole units
RGF	1.3752	6.182	619.7	8.7
RGD	1.3752	6.183	−598.1	−15.1
SGF	1.330	4.121	1,276.0	0.0
SGD	1.330	4.121	−1,303.0	0.0

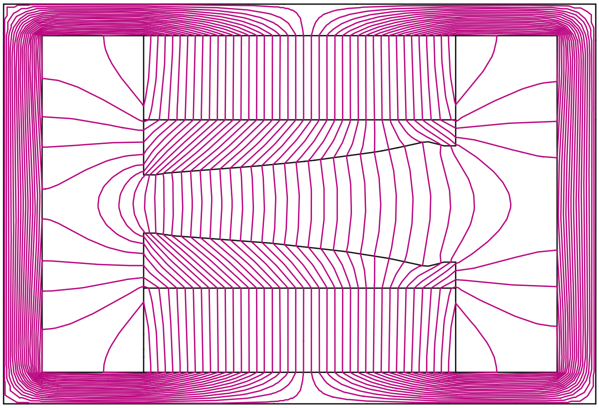

Fig. 3.18 Cross section of the Recycler ring gradient dipole magnet. Each of the magnet types was modeled using PANDRIA code from LANL

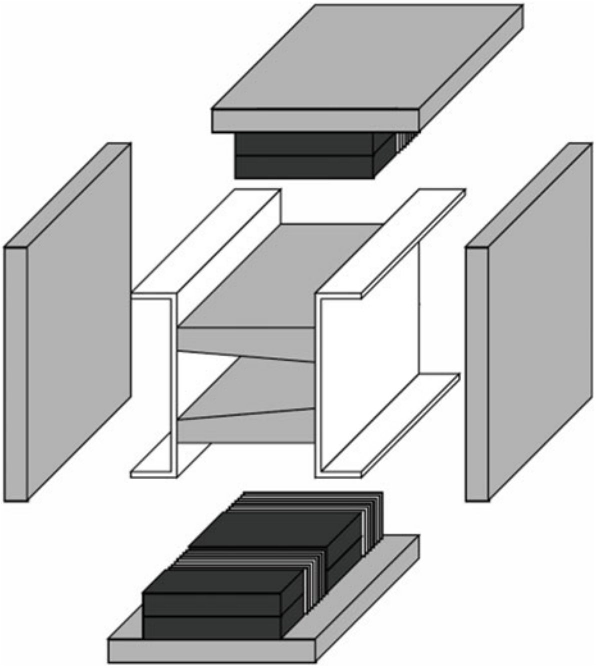

Fig. 3.19 Recycler permanent magnet gradient dipole components shown in an exploded view. For every 4″ wide brick there is an 0.5″ interval of temperature compensator material composed of 10 strips [14]

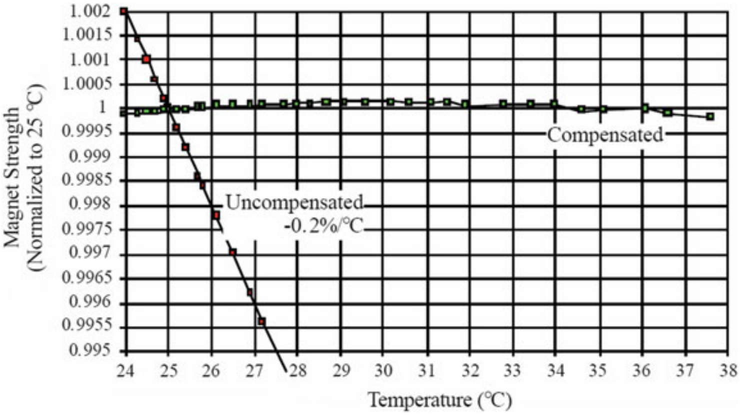

Fig. 3.20 Field strength vs. temperature for a stability test magnet using pre-production samples from the selected vendors for compensator alloy and ferrite

production. Due to the variable nature of the Curie point from heat to heat, the steel strips from different heats were randomly mixed. All Recycler magnets were frozen to 0 °C during the manufacturing process. The field for each magnet was measured at 0 °C and at 22 °C the amount of compensator steel was adjusted to keep the magnetic field in the 0.01 % tolerance. So, as a result the average magnetic field temperature stability of the Recycler magnets was about 0.004 %/°C rms over the operating range of 24–38 °C—see Fig. 3.20.

Long-term field stability was studied using the first production gradient magnet [38]. This magnet was measured with a Morgan (rotating) coil regularly over the first 2 years after its fabrication in November 1997. As seen in Fig. 3.21, the magnet lost a total of 0.1 % of initial strength in the first 2 years due to approximately logarithmic decay and has remained stable. The fact that over more than 6 years of the Recycler operations, its RF frequency of some 52 MHz has changed by less than 200 Hz is further proof that the magnetic field has remained stable within 0.04 %.

The longitudinal field for each gradient magnet was measured during production. It was determined that the field could be made more uniform by varying the number of compensator strips between each set of permanent magnets. More compensator strips were added at the quarter points of the magnet and fewer at the ends and middle. This served to keep the field flatter across the length of the magnet and to maintain the temperature compensation within the specified value of 0.01 %/°C.

To deal with the variation of the azimuthal magnetic field harmonics inevitable due to construction imperfections, each gradient magnet was measured with a Morgan (rotating) coil. Harmonics up to the 12-pole were measured. A FORTRAN program was written to calculate the shape of an end shim for each magnet that would adjust the quadrupole, skew quadrupole, sextupole, and octupole [39]. The program generated machine code for a wire EDM (Electric Discharge Machine) that cuts the exact shape required for each magnet. The shims were ready within

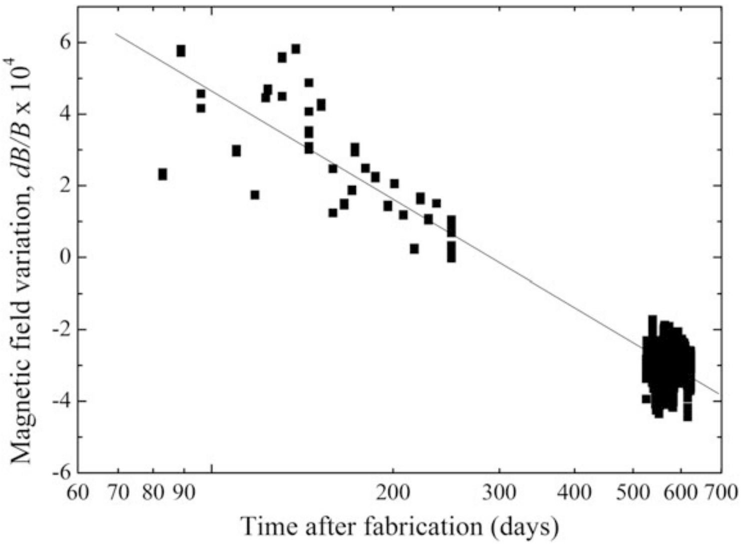

Fig. 3.21 Time evolution of the magnetic field in the Recycler gradient magnet (in the units of 10^{-4} of the main dipole field)

Table 3.2 Quadrupole magnet parameters

Magnet	Gradient (kG/m)	Focal length (1/m)	Gradient × length (kG)
RQMF	26.27	0.045	13.35
RQMD	−25.32	−0.043	−12.86
RQME	−21.97	−0.038	−11.16
RQEB	18.46	0.063	18.76
RQTF	16.68	0.029	8.47
RQTD	−16.87	−0.029	−8.57

24 h after the first measurement. In general, one iteration was required for each magnet. In rare cases two iterations were needed.

The poles of the Recycler quadrupole magnets [40] – see Table 3.2 – were made of type 1008 carbon steel. The hyperbolic shape of the poles was formed by cold extruding, no other machining of the poles was required. Strontium ferrite bricks were placed behind the poles. In the corners, steel washers were added to adjust the gradient, the skew quad, sextupole, and octupole field components. Steel washers were attached to the face of the poles to eliminate the 12-pole component (Table 3.2).

Special magnets needed for the beam injection and extraction—Lambertsons magnets and mirror magnets—were also made with strontium ferrite [41]. The base of the Lambertson magnets was made of solid steel. The hole for the field free region was gun bored then through entire 4 m length. This provided for a field free region of less than 5 G with a field region of 0.16 T. The use of solid base plates was allowed for a common design for all five Lambertson magnets but different configuration of the bending field.

With experience of operation it became clear that small corrector magnets such as skew quadrupoles and sextapoles were required. Several of these magnets were fabricated to solve specific problems [42]. Both strontium ferrite and samarium cobalt permanent magnets were used.

References

1. E.L. Hubbard (ed.), *Booster Synchrotron*, FERMILAB-TM-0405, Batavia, IL, 1973
2. E.J. Prebys et al., New corrector system for the Fermilab booster, in *Proceedings of IEEE PAC07*, Albuquerque, NM, 2007, p. 467
3. W. Pellico, New booster multi-pole correctors commissioning. Presentation to the Fermilab all experimenters meeting, Batavia, IL, 11 October 2010
4. J. Lackey et al., Operation and performance of the new Fermilab booster H-injection system, in *Proceedings of IEEE PAC07*, Albuquerque, NM, 2007, p. 1709
5. C. Hojvat et al., The multiturn charge exchange injection system for the Fermilab booster accelerator. IEEE Trans. Nucl. Sci. **NS-26**(3), 3149 (1979)
6. D. McGinnis, Status of the Fermilab booster after the 400 MeV upgrade, in *Proceedings of EPAC1994*, London, England, 1994, p. 497
7. W. Chou et al., Fermilab booster modeling and space charge study, in *Proceedings of IEEE PAC03*, Portland, OR, 2003, p. 2925
8. F.T. Cole (ed.), *Design Report National Accelerator Laboratory*, Oak Brook, IL, January 1968
9. F.T. Cole (ed.), *Design Report Tevatron 1 Project*, Batavia, IL, 1984
10. P.S. Martin (ed.), *The Fermilab Main Injector Technical Design Report*, Batavia, IL, 1995
11. D.J. Harding et al., Strength and shape of the magnetic field of the Fermilab main injector dipoles, in *Proceedings of IEEE PAC09*, New York, NY, 1999, p. 3318, and references therein
12. D.J. Harding et al., Magnetic field strength and shape measurements of the Fermilab main injector quadrupoles, in *Proceedings of IEEE PAC97*, Vancouver, BC, 1997, p. 3269
13. W. Chou et al., Operational aspects of the main injector large aperture quadrupole (WQB), in *Proceedings of IEEE PAC07*, Albuquerque, NM, 2007, p. 1685
14. G.P. Jackson (ed.), *Fermilab Recycler Ring, Technical Design Report*, FERMILAB-TM-1991, 1996
15. F.T. Cole et al. (eds.), *A Report on the Design of the Fermi National Accelerator Laboratory Superconducting Accelerator*, Batavia, IL, 1979
16. A.V. Tollestrup, *The Amateur Magnet Builder's Handbook*, Fermilab-UPC-086, Batavia, IL, 1979
17. N.M. Gelfand, Tune drifts on the Tevatron front porch, in *Proceedings of PAC07*, Albuquerque, NM, 2007, p. 1691
18. R. Hanft, B. Brown, D. Herrup, M. Lamm, A. McInturff, M. Syphers, Fermilab Preprint TM-1542, 1988
19. K.-H. Mess, P. Scmusser, S. Wolff, *Superconducting Accelerator Magnets* (World Scientific Publishing Co. Pte. Ltd., Singapore, 1996)
20. D. Herrup et al., Phys. Rev. E **49**(6), 5660 (1994)
21. D. Finley, D. Edwards, R. Hanft, R. Johnson, A. McInturff, J. Strait, Fermilab Preprint FN-451, 1987
22. J. Annala et al., in *Proceedings of 2005 IEEE Particle Accelerator Conference*, Knoxville, TN, 2005, p. 54
23. J. Volk et al., Tevatron alignment issues 2003–2004, in *Proceedings of 2005 IEEE Particle Accelerator Conference*, Knoxville, TN, 2005, p. 2146
24. J. Holt et al., Calculating luminosity for a coupled Tevatron lattice, in *Proceedings of 1995 IEEE Particle Accelerator Conference*, Dallas, TX, 1996, p. 456

25. N. Gelfand, Coupling in the Tevatron, in *Proceedings of 1995 IEEE Particle Accelerator Conference*, Dallas, TX, 1996, p. 452
26. M. Syphers, Strong systematic steering correction in regions of the Tevatron, Fermilab Internal Report Beams-doc-491, 2003
27. M. Syphers, D. Harding, Deterioration of the skew quadrupole moment in Tevatron dipoles over time, in *Proceedings of 2005 IEEE Particle Accelerator Conference*, Knoxville, TN, 2005, p. 1967
28. M. Syphers et al., Observations of strong transverse coupling in the Tevatron, in *Proceedings of 2005 IEEE Particle Accelerator Conference*, Knoxville, TN, 2005, p. 2029
29. E. Caulfield, *Investigation of Creep Behavior of the Glass Reinforced Composite Stand-Offs* (Packer Engineering Associates Inc., New York, NY, 1981)
30. G. Kobliska to D. Harding, private communication
31. M. Syphers, Skew Quadrupole tuning and vertical dispersion in the Tevatron, Fermilab Beams-doc-611, 2003
32. G. Ambrosio et al., Results of an investigation of the skew quadrupole issue in Tevatron dipoles, Fermilab Internal Note TD-03-045, 2003
33. R. Hanft et al., Magnetic field properties of Fermilab energy saver dipoles, in *Proceedings of 1983 IEEE Particle Accelerator Conference*, Santa Fe, NM, 1983, p. 3381
34. J. Blowers et al., Reshimming of Tevatron dipoles: a process-quality and lessons-learned perspective, in *Proceedings of 2005 IEEE Particle Accelerator Conference*, Knoxville, TN, 2005, p. 3156
35. G.W. Foster, in *Proceedings of 1995 IEEE Particle Accelerator Conference*, Dallas, TX, 1995, pp. 1298–1300
36. G.W. Foster et al., in *Proceedings of 1998 European Particle Accelerator Conference*, Stockholm, Sweden, 1998, pp. 189–193
37. H.D. Glass et al., in *Proceedings of 1997 IEEE Particle Accelerator Conference*, Vancouver, BC, 1997, p. 3260–3262
38. J. Volk, J. Instrum. **6**, T08003 (2011)
39. G.W. Foster et al., in *Proceedings of 1999 IEEE Particle Accelerator Conference*, New York, NY, 1999, pp. 3324–3326
40. H.D. Glass et al., in *Proceedings of 1997 IEEE Particle Accelerator Conference*, Vancouver, BC, 1997, pp. 3286–3287
41. G.W. Foster et al., in *Proceedings of 1997 IEEE Particle Accelerator Conference*, Vancouver, BC, 1997, pp. 3280–3282
42. J. Volk et al., in *Proceedings of 2003 IEEE Particle Accelerator Conference*, Portland, OR, 2003, pp. 1766–1768
43. S.D. Holmes, V.D. Shiltsev, The legacy of the Tevatron in the area of accelerator science. Annu. Rev. Nucl. Part. Sci. **63**, 435–465 (2013)